# Second-harmonic generation at angular incidence in a negative-positive index photonic band-gap structure

Giuseppe D'Aguanno,[1,*] Nadia Mattiucci,[2] Michael Scalora,[1] and Mark J. Bloemer[1]
[1]*Charles M. Bowden Research Center, RDECOM Building 7804, Redstone Arsenal, Alabama 35898-5000, USA*
[2]*Time Domain Corporation, Cummings Research Park, 7057 Old Madison Pike Huntsville, Alabama 35806, USA*
(Received 9 May 2006; revised manuscript received 14 July 2006; published 23 August 2006)

In the spectral region where the refractive index of the negative index material is approximately zero, at oblique incidence, the linear transmission of a finite structure composed of alternating layers of negative and positive index materials manifests the formation of a new type of band gap with exceptionally narrow band-edge resonances. In particular, for TM-polarized (transverse magnetic) incident waves, field values that can be achieved at the band edge may be much higher compared to field values achievable in standard photonic band-gap structures. We exploit the unique properties of these band-edge resonances for applications to nonlinear frequency conversion, second-harmonic generation, in particular. The simultaneous availability of high field localization and phase matching conditions may be exploited to achieve second-harmonic conversion efficiencies far better than those achievable in conventional photonic band-gap structures. Moreover, we study the role played by absorption within the negative index material, and find that the process remains efficient even for relatively high values of the absorption coefficient.

DOI: 10.1103/PhysRevE.74.026608 PACS number(s): 42.65.−k

## I. INTRODUCTION

Within the past few years, a new class of artificial materials has captured the interest of the scientific community. Known as left-handed or negative index materials (NIMs), these materials simultaneously display negative permittivity and magnetic permeability [1–3]. The most impressive property of NIMs may well be their ability to refract the light in the opposite way with respect to what an ordinary materials does [4] due to a negative refractive index, and several applications have been proposed. Arguably the most important is the possibility to construct a "perfect" lens, i.e., a lens that can also focus evanescent, near-field waves emanating from a source located near a NIM [1]. Other applications have also been envisioned, and they include but are not limited to the possibility to have dispersion free-pulse propagation in a single slab of NIM [5], as well as broadband omnidirectional reflection [6,7]. The nonlinear properties of a single slab of NIM have been investigated in the context of gap-soliton formation [8] mediated by a cubic nonlinearity, and bistability [9]. In bulk materials, a modified nonlinear Schrödinger equation that includes the effects of a dispersive permeability has been derived [10], and its stability has been studied in the ultrashort pulse limit [11]. Defect-induced nonlinear transmission of a periodic structure created by alternating slabs of two materials with positive and negative refractive index has also been studied [12]. Quadratic phenomena have also been investigated in bulk NIMs, second-harmonic generation (SHG), in particular [13–15]. One-dimensional structures made of alternating layers of negative and positive index materials (NIM/PIM), have also received some attention due to their peculiar properties. It has been theoretically predicted [16] and experimentally verified [17] that such structures open a Bragg gap around the spectral region where the index of refraction averages to zero inside the elementary cell. This so-called zero-$\bar{n}$ Bragg gap is unique because it cannot be replicated in ordinary materials, and its properties are different compared to conventional Bragg gratings made of PIMs. For example, strong beam modification and reshaping of tunneling pulses have been predicted [18], while the location and depth of the gap are relatively insensitive to disorder [16] and to the incident angle [19]. In the nonlinear regime, it has also been shown that this zero-$\bar{n}$ Bragg gap can support omnidirectional gap solitons in the presence of a Kerr nonlinearity [20]. SHG in NIM/PIM structures has been less studied, but the possibility of interface SHG occurring in standard, centrosymmetric materials near the zero-$\bar{n}$ gap has been predicted [21], and a study of coupled cavities composed of nonlinear PIMs and linear NIMs has also been carried out [22].

In this paper we study SHG at an oblique incidence from a NIM/PIM Bragg grating. We show that in the spectral region where the refractive index of the negative index material is approximately zero, a new type of gap forms, one that has different properties with respect to the zero-$\bar{n}$ gap. This new gap is characterized by exceptionally narrow band-edge transmission resonances, and extremely high field localization properties for an incident TM field. We exploit high field localization together with the availability of perfect phase matching conditions due to the periodicity of the structure in order to achieve a highly efficient SHG compared to traditional photonic band-gap (PBG) structures.

## II. LINEAR PROPERTIES

Let us start our analysis with Fig. 1 where we show the transmission at normal incidence of a $N=6$ period, NIM/PIM Bragg grating. The permittivity and the magnetic permeability of the NIM are described by a lossy Drude model [23]:

*Corresponding author. Fax: 001-256-8422507;
Electronic address: giuseppe.daguanno@us.army.mil or giuseppe.daguanno@gmail.com

 

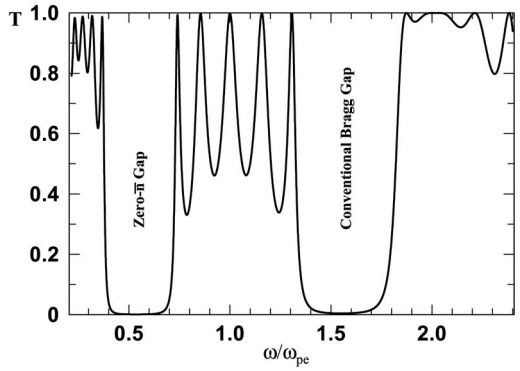


FIG. 1. Transmission vs normalized frequency $\omega/\omega_{\mathrm{pe}}$ at normal incidence for $N=6$ periods of alternating NIM/PIM layers. The thicknesses of the layers are $a=b=0.1\lambda_{\mathrm{pe}}$, and $\lambda_{\mathrm{pe}}=2\pi c/\omega_{\mathrm{pe}}$ is the electric plasma wavelength. The PIM is assumed to be a nondispersive material with $n_{\mathrm{PIM}}=2.5$. The dispersion of the NIM is described by a lossy Drude model with $\omega_{\mathrm{pe}}=\omega_{\mathrm{pm}}$, as detailed in the main text. The structure is surrounded by air.

$\varepsilon_{\mathrm{NIM}}(\tilde{\omega})=1-1/[\tilde{\omega}(\tilde{\omega}+i\tilde{\gamma}_e)]$, $\mu_{\mathrm{NIM}}(\tilde{\omega})=1-(\omega_{\mathrm{pm}}/\omega_{\mathrm{pe}})^2/[\tilde{\omega}(\tilde{\omega}+i\tilde{\gamma}_m)]$, where $\tilde{\omega}=\omega/\omega_{pe}$ is the normalized frequency, $\omega_{pe}$ and $\omega_{pm}$ are the respective electric and magnetic plasma frequencies, and $\tilde{\gamma}_e=\gamma_e/\omega_{pe}$ and $\tilde{\gamma}_m=\gamma_m/\omega_{pe}$ are the corresponding electric and magnetic loss terms normalized with respect to the electric plasma frequency. In our case we assume that $\omega_{pm}=\omega_{pe}$ and $\tilde{\gamma}_e=\tilde{\gamma}_m=\gamma=10^{-4}$. We note that for $\omega_{pm}=\omega_{pe}$ the complex refractive index of the NIM $\hat{n}_{\mathrm{NIM}}$, the permittivity and the magnetic permeability are equal, i.e., $\hat{n}_{\mathrm{NIM}}=\varepsilon_{\mathrm{NIM}}=\mu_{\mathrm{NIM}}$. The details of the structure are described in the figure caption. For simplicity, we assume that the structure is surrounded by air. The dispersion of the NIM material is such that its refractive index is approximately zero for a frequency near the electric plasma frequency, i.e., $n_{\mathrm{NIM}}\cong 0$ at $\tilde{\omega}\cong 1$. Moreover, $n_{\mathrm{NIM}}<0$ for $\tilde{\omega}<1$, and $n_{\mathrm{NIM}}>0$ for $\tilde{\omega}>1$. The PIM is assumed to be a standard dielectric material with a refractive index $n_{\mathrm{PIM}}=2.5$. The figure shows that the structure admits two gaps: the zero-$\bar{n}$ gap, centered around $\tilde{\omega}\cong 0.5$; the second order gap is the first conventional Bragg gap. In the spectral region between the two gaps there is a pass band characterized by Fabry-Perot like transmission resonances. In Figs. 2(a) and 3(a) we depict the transmission function for both TE (transverse electric) and TM (transverse magnetic) polarizations, for incidence angles of $\theta_{\mathrm{i}}=15°$ [Fig. 2(a)] and $\theta_{\mathrm{i}}=30°$ [Fig. 3(a)], respectively. In Figs. 2(b) and 3(b) we show the magnification of the transmission function around the respective band gaps, finally in Fig. 2(c) and 3(c) we show the corresponding reflectance ($R$). As one may expect, the position and the width of the zero-$\bar{n}$ gap remain relatively insensitive to the incident angle and polarization of light [16,19]. What is remarkable here is the formation of a new gap, centered in the region around $\tilde{\omega}\cong 1$, which is shown magnified in the inset of the figures. In contrast to the zero-$\bar{n}$ gap, this gap is quite sensitive to the incident angle, and widens almost symmetrically around the point $\tilde{\omega}\cong 1$ for increasing angles of incidence, as Figs. 2 and 3 show. Moreover, we can say, looking at the corresponding reflectances shown in Figs. 2(c) and 3(c), that this angular gap is a true mirrorlike one with $R>0.99$ at the center of the gap. We

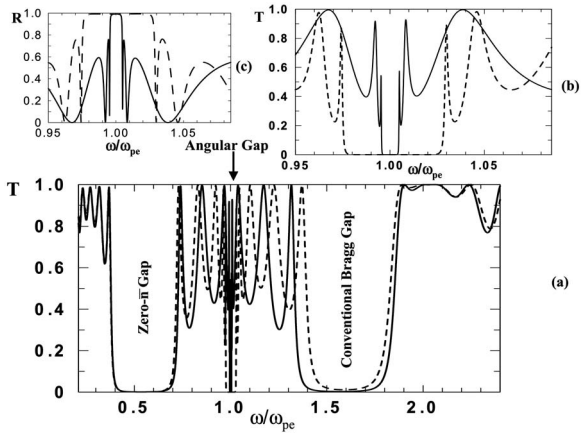


FIG. 2. Main figure: TE (solid line) and TM (dashed line) transmission at an incident angle of 15° for the same structure described in Fig. 1. Upper figure on the right: Magnification of the angular gap and of the band-edge transmission resonances. Upper figure on the left: Reflectance around the angular band gap.

point out that in this case we have used a rather small absorption coefficient ($\tilde{\gamma}_e=\tilde{\gamma}_m=\gamma=10^{-4}$), nevertheless our calculations show that the mirrorlike behavior remains dominant up to values of the absorption coefficient of the order of $10^{-2}$ for which the reflectance $R$ at the center of the gap drops to $R\sim 0.8$. The gap appears to be wider for TM than for TE polarization. The widening of this gap should also be contrasted with the behavior of a conventional Bragg gap, that actually blueshifts for increasing angles of incidence. Note also that the band-edge transmission resonances are exceptionally narrow, considered that the structure is composed of only $N=6$ periods. The physical mechanism behind the formation of this gap is simple. Keeping in mind that we are operating in a region where the refractive index of the NIM is less than one in absolute value, i.e., $|n_{\mathrm{NIM}}|<1$, while the refractive index of the surrounding medium (air) is 1, it is evident that evanescent modes will be created in the NIM layers due to total internal reflection in air when the angle of the incoming radiation roughly satisfies the following condition: $|\sin\theta_{\mathrm{i}}/n_{\mathrm{NIM}}|\geqslant 1$. Now, a unique interplay between the evanescent modes formed within the NIM layers due to total reflection in air, and the multiple interference typical of PBG

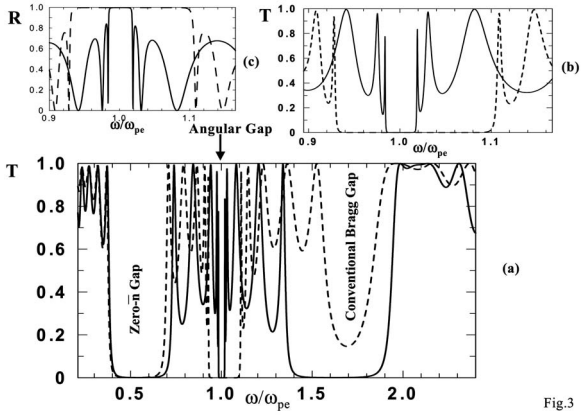


FIG. 3. Same as in Fig. 2 at an incident angle of 30°.

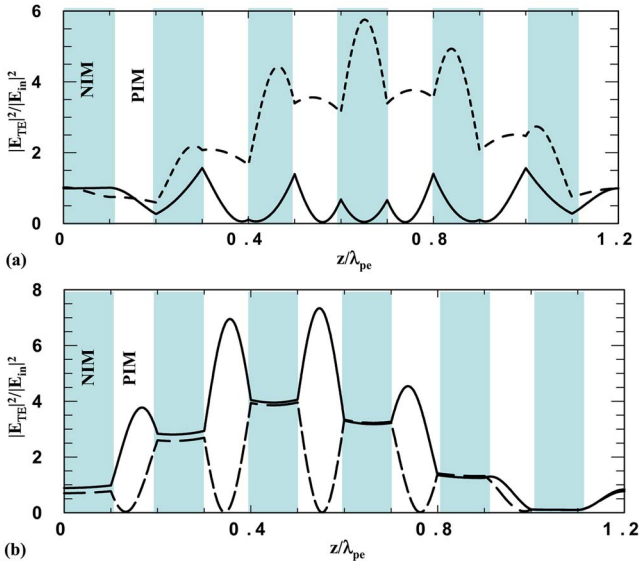


FIG. 4. (Color online) (a) Localization of the electric field incident at 30°, TE polarized, inside the structure, respectively, at the low frequency band-edge transmission resonance of the zero-$\bar{n}$ gap (dashed line) and at the high frequency (solid line). (b) Same as in (a) for the field tuned at the band-edge transmission resonances of the angular gap. The fields inside the structure are normalized with respect to the amplitude of the incident field.

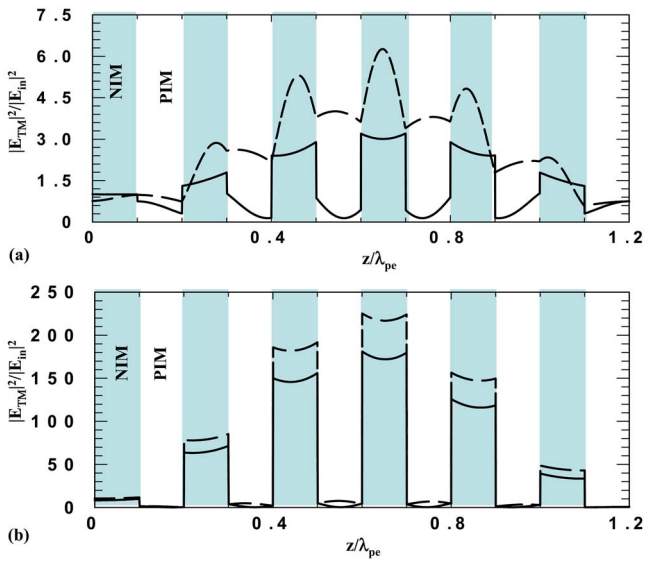


FIG. 5. (Color online) Same as in Fig. 4 for a TM polarized incident field.

structures, gives rise to the kind of gap that we are analyzing here. The phenomenon of total internal reflection also qualitatively explains why the gap widens [6,7] instead of blueshifting, as is the case for a conventional Bragg gap. We point out that, although in the region where the gap is formed the refractive index of the NIM is near zero, its behavior should not be compared to what occurs in a metal. In fact, had its behavior been metallicklike, we would have had a region of high reflectivity around $\tilde{\omega} \cong 1$ even at normal incidence. From Fig. 1, one may easily ascertain that at $\tilde{\omega}=1$ the reflectivity goes to zero, i.e., $R=0$ and $T=1$, along with the formation of a pass band, with Fabry-Perot-like transmission resonances generated by multiple interference effects. Put another way, at normal incidence the NIM behaves as a perfectly transparent material. We may draw some conclusions also by analyzing the expression for the reflectivity at the interface between air and a semi-infinite, generic, magnetic material: $R=|(\hat{n}/\mu-1)/(\hat{n}/\mu+1)|^2$. In our case, $R=0$ because $\hat{n}_{\mathrm{NIM}}=\varepsilon_{\mathrm{NIM}}=\mu_{\mathrm{NIM}}$, and the impedance of the NIM is perfectly matched with the impedance of the air. For typical metals, on the other hand, we have a high reflection coefficient, i.e., $R \cong 1$.

The above-mentioned behavior makes the new gap we are describing qualitatively different from the so-called "intrinsic zero-$n$ gap," which is instead formed at normal incidence, in the region between the electric and magnetic plasma frequency, and which also displays metallic behavior [6–8,22,24]. In Fig. 4(a) we show the localization for incident fields, TE polarized, at $\theta_i=30°$ tuned, respectively, at the low frequency (dashed line) and high frequency (solid line) band-edge transmission resonances of the zero-$\bar{n}$ gap shown in Fig. 3, while in Fig. 4(b) they are tuned, respectively, at the low and high frequency band-edge transmission resonances of the angular gap also shown in Fig. 3.

In Figs. 5(a) and 5(b) we show the localization properties for TM-polarized fields also at the band-edge resonances. What is remarkable here is that the local value of the square modulus of the field in the central layers of NIM is approximately two orders of magnitude greater than its value at the input [Fig. 5(b)]. This is an impressive result, recalling that the structure is only of six periods in length. There are two concomitant effects that conspire to achieve this exceptionally high field localization inside the NIM layers. First, the real part of the permittivity $\varepsilon_R$ inside the NIM at both the high and low frequency band edges are $\varepsilon_{R,\mathrm{NIM}} \sim 0.16$ (high frequency) and $\varepsilon_{R,\mathrm{NIM}} \sim -0.14$ (low frequency), respectively. For the PIM we have $\varepsilon_{\mathrm{PIM}}=(2.5)^2$. Now, the continuity of the component of the electric displacement vector orthogonal to the interfaces requires that $E_{\perp \mathrm{NIM}} \sim E_{\perp \mathrm{PIM}} \varepsilon_{\mathrm{PIM}}/\varepsilon_{R,\mathrm{NIM}}$. Therefore, the electric field inside the NIM has the potential of being significantly enhanced by a factor of $|\varepsilon_{\mathrm{PIM}}/\varepsilon_{R,\mathrm{NIM}}| \sim 40$ with respect to the electric field present in the PIM. Of course, this enhancement factor would be accurate only in the case of static fields, or in the case of a single interface between two semi-infinite materials. In our case, the second factor that contributes is interference in the form of multiple reflections within the structure, which on one hand mitigates the enhancement factor calculated above, while on the other hand force the field into a bell-shaped envelope across the structure, which is typical of an incident field tuned at the band-edge transmission resonances of conventional PBG structures. Therefore, while the end result here appears to be field enhancement just as in ordinary PBGs, the route to high local field localization is qualitatively different.

The idea is to take advantage of the high TM field localization at the transmission resonances in order to efficiently generate SH. Of course, field localization is just one of the two key concepts that allow us an efficient process; the second is the availability of phase matching conditions. As we

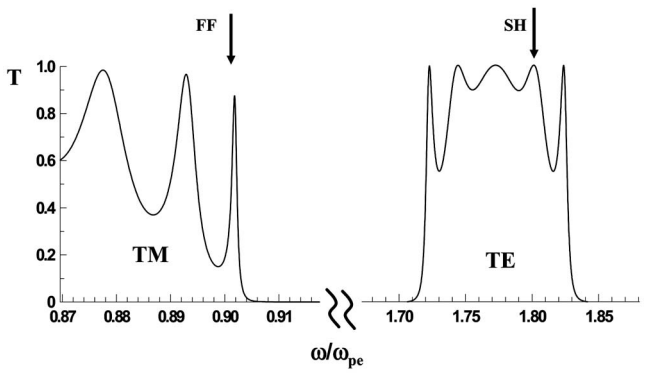


FIG. 6. TM and TE transmission vs normalized frequency $\omega/\omega_{pe}$ for an angular incidence of 30°. The structure is made of $N=6$ periods of alternating NIM/PIM layers. The thicknesses of the layers are $a=b=0.3\lambda_{pe}$, for a total length of $L=3.6\lambda_{pe}$. The PIM is assumed to be a normal dispersive material having linear dispersion between the FF and the SH frequency. Here we have $n_{PIM,FF}\cong 2.4705$ and $n_{PIM,SH}\cong 2.8823$. The dispersion of the NIM is described by a lossy Drude model with $\omega_{pe}=\omega_{pm}$, as detailed in the main text. The structure is surrounded by air. The arrows indicate the tuning of the FF pump field which is TM-polarized and the tuning of the SH generated field which is TE-polarized.

will see in the next section both high field localizations and phase matching conditions are simultaneously available in the kind of structures we are considering here.

## III. SECOND-HARMONIC GENERATION

In order to study SHG, in Fig. 6 we show the linear transmission at 30° and the tuning conditions for a structure of $N=6$ periods of NIM/PIM alternating layers. The NIM has the same permittivity and magnetic permeability functions as used in the previous section and we suppose that it possesses a quadratic nonlinearity. The PIM is considered a generic dielectric material with no quadratic nonlinearity and with linear dispersion between the FF and SH frequency. In particular, we take $n_{PIM,FF}\cong 2.4705$ and $n_{PIM,SH}\cong 2.8823$ which corresponds to a dispersion between the FF and the SH of approximately 17%. The details of the structure are described in the caption of the figure. The FF field is TM polarized and it is tuned at the low frequency transmission resonance of the angular gap where $\omega/\omega_{pe}\cong 0.9018$ and the refractive index of the NIM is approximately $n_{NIM}\cong -0.23$. Here we suppose for simplicity that the SH emitted is TE polarized, i.e., we are considering a TM→TE process. The dispersion used for the PIM makes possible tuning the SH field at the second transmission resonance near the second conventional Bragg gap. The reason for this tuning can be easily understood if we plot the Bloch vector $K_\beta$ of the elementary cell of the structure (see Fig. 7). Momentum conservation requires in our case that $\Delta K_\beta = K_{\beta,TE}(2\omega) - 2K_{\beta,TM}(\omega)\cong G_m$, where $G_m=2\pi m/\Lambda$ is one of the reciprocal lattice vectors, $\Lambda=a+b$ is the length of the elementary cell, and $m$ is an integer number. Now, from Fig. 7 we see that tuning the FF at the band edge transmission resonance of the angular gap results in a Bloch vector $K_{\beta,TM}(\omega)$

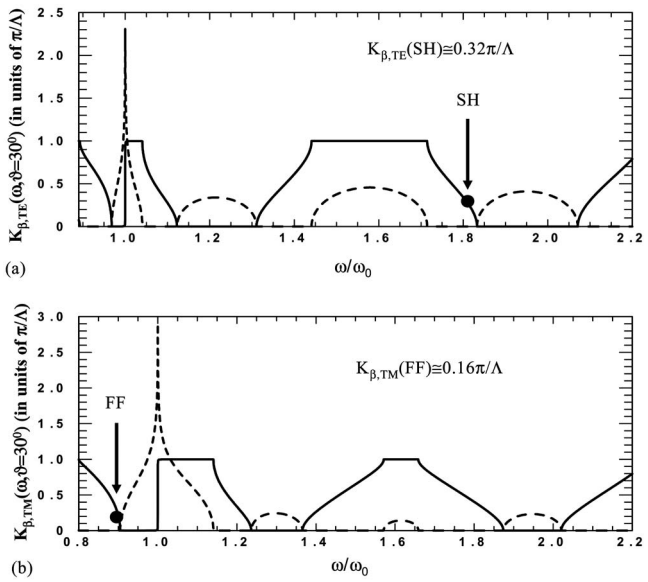


FIG. 7. (a) Real (solid line) and imaginary part (dashed line) of the TE Bloch vector vs $\omega/\omega_{pe}$ for an incident angle of 30°. The Bloch vector is calculated for the elementary cell of the structure described in Fig. 6, which has length $\Lambda=a+b$. (b) Same as (a) for TM. The arrows indicate the tuning of the FF and SH field. Note that for this tuning conditions we have momentum quasiconservation, i.e., $\Delta K_\beta = K_{\beta,TE}(2\omega) - 2K_{\beta,TM}(\omega)\cong 0$.

$\cong 0.16\pi/\Lambda$ while tuning the SH at the second transmission resonance near the second conventional band-gap results in a Bloch vector that is approximately double, i.e., $K_{\beta,TE}(2\omega)\cong 0.32\pi/\Lambda$, and therefore momentum quasiconservation, i.e., $\Delta K_\beta\cong 0$, is achieved. In Fig. 8 we show the localization properties of the FF field. The FF field lays in the incidence plane and it can be decomposed into the sum of two vectors:

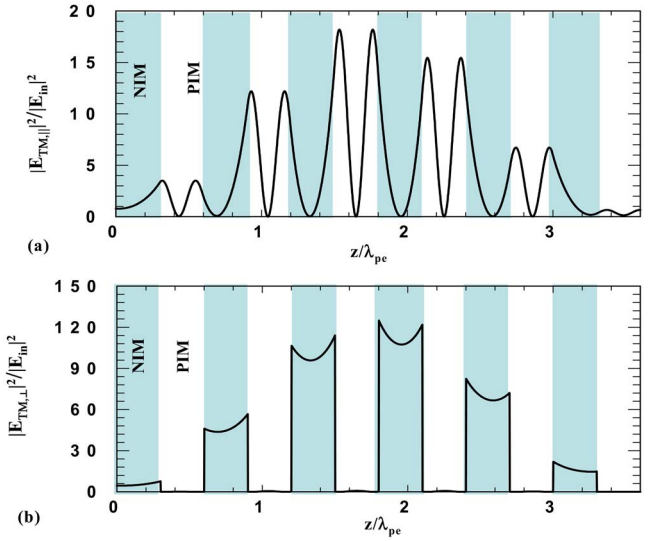


FIG. 8. (Color online) (a) Localization inside the structure of the component of the FF field parallel to the interfaces. (b) Localization of the component of the FF field orthogonal to the interfaces. The fields are normalized with respect to the amplitude of the incident field.

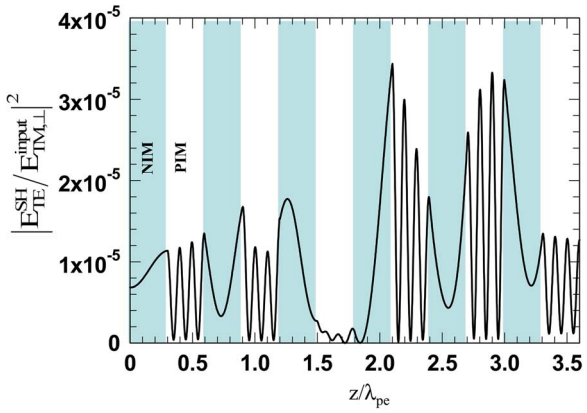


FIG. 9. (Color online) SH field generated inside the structure for $d^{(2)}E_{\mathrm{TM},\perp}^{(\mathrm{input})}=10^{-5}$. We suppose that only the NIM layers posses a quadratic nonlinearity.

$\mathbf{E}_{\mathrm{TM}}=\mathbf{E}_{\mathrm{TM},\parallel}+\mathbf{E}_{\mathrm{TM},\perp}$ where $\mathbf{E}_{\mathrm{TM},\parallel}$ [see Fig. 8(a)] is the electric field component parallel to the interfaces of the multilayered structure and $\mathbf{E}_{\mathrm{TM},\perp}$ [see Fig. 8(b)] is the component orthogonal to the interfaces. Note that the high field localization of the FF field over the NIM layers is mostly attributable to its orthogonal component, i.e., $\mathbf{E}_{\mathrm{TM},\perp}$. In what follows we suppose for simplicity that the quadratic nonlinearity of the NIM couples only with the orthogonal component of the FF field and we suppose also that it generates a TE-polarized SH signal, i.e., $E_{\mathrm{SH,TE}}\sim d^{(2)}E_{\mathrm{TM},\perp}^2$, where $d^{(2)}$ is the quadratic coupling coefficient of the NIM.

In Fig. 9 we show the SH field generated inside the structure for an input FF field so that $d^{(2)}E_{\mathrm{TM},\perp}^{(\mathrm{input})}=10^{-5}$. Note that we are supposing a rather low value of the quadratic nonlinearity and a moderate value of the input intensity, in fact, if one considers a nonlinear coupling coefficient of 1 pm/V the strength of the orthogonal component of the incident field should be $10^7$ V/m, which corresponds to an intensity of approximately 13 MW/cm$^2$. The calculation of the SH generated inside the structure has been performed using a rigorous Green function approach [25], calculated at an angular incidence as in Ref. [26] and extended to treat magnetic active materials as detailed in Ref. [22]. In Fig. 10 we calculate the SH emitted both in the forward and in the backward direction as a function of the refractive index of the PIM at

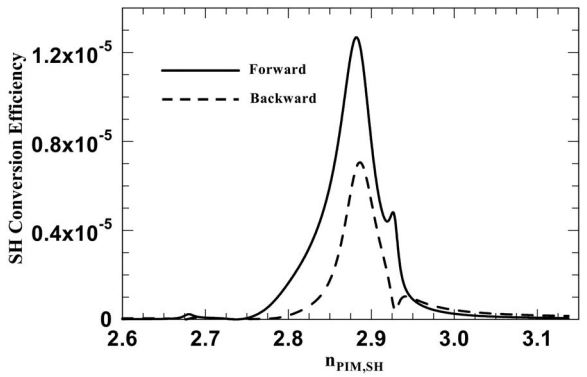


FIG. 10. SH conversion efficiency $\eta$ vs the refractive index of the PIM layers at the SH, $n_{\mathrm{SH,PIM}}$.

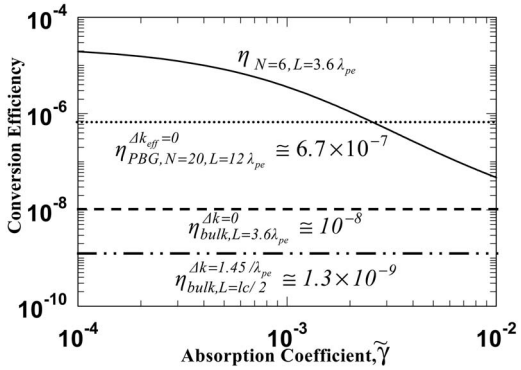


FIG. 11. Total (forward+backward) conversion efficiency vs the absorption coefficient of the NIM (solid line). Conversion efficiency (dotted line) of a nonabsorbing, conventional PBG structures made of $N=20$ periods alternating layers of a generic dielectric material and air. The thickness are, respectively, $0.35\lambda_{\mathrm{pe}}$ (dielectric material) and $0.25\lambda_{\mathrm{pe}}$ (air) for a total length of $L=12\lambda_{\mathrm{pe}}$. The dielectric material is considered with a linear dispersion. The refractive index at the FF is 1.428 57 and at the SH frequency is 1.5179. The FF field is tuned at the low frequency transmission resonance of the first Bragg gap while the SH field is tuned at the second transmission resonance on the low frequency side of the second band gap. Those tuning conditions lead to a phase-matched SHG. Conversion efficiency (dashed line) of a perfect phase matched, nonabsorbing, bulk material with the same length of the NIM/PIM structure. The bulk is assumed to have a refractive index of 1.6. Conversion efficiency (dotted and dashed line) for the same bulk material but having an 8% dispersion in the refractive index between the FF and SH frequency. In this case we take $L=l_c/2$ where $l_c$ is its coherence length.

the SH frequency. We find that the maximum SH emission is achieved when the refractive index of the PIM at the SH frequency is approximately $n_{\mathrm{PIM,SH}}\cong 2.8823$ which corresponds to tuning the SH field at the second transmission resonance near the second conventional band gap as described in Fig. 6, in agreement with the momentum conservation described in Figs. 7.

We would like to underline that, as we have already stated in Sec. II, in our calculations the absorption coefficient of the NIM for both the electric and magnetic part has been set to $\tilde{\gamma}_e=\tilde{\gamma}_m=\gamma=10^{-4}$. Of course, increasing the value of the absorption coefficient would result in the lowering of the transmission resonances which ultimately leads to decrease the SH conversion efficiency. Although recent advancements in the field of metamaterials suggest that NIMs operating in the mid and near infrared regime, which are the regimes to which we are referring here, may be within reach [27–32], still the issue of the absorption and/or loss may represent a serious obstacle for several practical applications including the one we are proposing in this paper. In order to tackle this issue, in Fig. 11 we have therefore calculated the SH emission as function of the absorption coefficient, by increasing the absorption coefficient of two orders of magnitude, i.e., passing from $\gamma=10^{-4}$ to $\gamma=10^{-2}$. An absorption coefficient of $\gamma=10^{-2}$ corresponds in our case to an extinction coefficient ($K$) that is still of the same order of magnitude ($K\sim 10^{-2}$) at the FF. This value can be considered large, given

the fact that typical metals, such as silver (Ag) in the visible range, for example, have extinction coefficients of the order of the unity ($K \sim 1$) [33], and nonabsorbing dielectric materials, such as glass, for example, have extinction coefficients of the order of $K \sim 10^{-7}$ or less. The SH emission is calculated for the tuning condition described in Fig. 6, which represents the optimal condition for SHG. In order to get a sense of the exceptionally high conversion efficiency achievable in this structure we have reported for comparison the SHG generated from three *nonabsorbing* structures which are the following: (a) a $N=20$ period conventional PBG structure in perfect effective phase matching and with the nonlinearity in the high index layer [34–36]; (b) a perfectly phase matched bulk material of the same length as our structure; (c) a bulk material with 8% dispersion in the refractive index between the FF and the SH frequency, and thickness equal to half of its coherence length ($l_c$) in order to maximize the SH emitted. In all cases the product of the input field times the nonlinear coupling coefficient has been set to $10^{-5}$, i.e., $d^{(2)}E^{(\text{input})}=10^{-5}$, as for the NIM/PIM structure. The figure shows that the conversion efficiency of the $N=6$ period NIM/PIM structure is greater than that of the phase matched, $N=20$ period, conventional, nonabsorbing PBG structure for values of the absorption coefficient smaller or approximately equal to $2.5\times10^{-3}$, i.e., $\gamma \leqslant 2.5\times10^{-3}$. In the case of $\gamma = 10^{-4}$ the conversion efficiency of the NIM/PIM structure is approximately 40 times better than that achievable in the PBG structure. Those results are very impressive, considering that the NIM/PIM structure is only of 6 periods and $3.6\lambda_{\text{pe}}$ in length, while the PBG structure is 20 periods and $12\lambda_{\text{pe}}$ in length. If we also compare the total quantity of nonlinear material present in the structure ($L_{d^{(2)}}$) we realize that $L_{d^{(2)}}^{NIM/PIM}=1.8\lambda_{pe}$ and $L_{d^{(2)}}^{PBG}=7\lambda_{pe}$. Now, considering the conversion efficiency per square length of nonlinear material ($\eta/(L_{d^{(2)}})^2$), we can say that the NIM/PIM structure is always more efficient than the PBG structure as long as the absorption coefficient $\gamma \leqslant 10^{-2}$, if the respective conversion efficiencies per square length of nonlinear material are compared.

## IV. CONCLUSIONS

In conclusion we have studied SHG in a NIM/PIM, finite, $N=6$ periods, PBG structure with the pump field TM polarized, tuned at the band-edge transmission resonance of the angular gap. We have shown that the simultaneous availability of exceptionally high field localizations and phase matching conditions conspire to yield conversion efficiencies far better than those achievable in standard, positive index PBG structures. We have also studied the detrimental role played by the absorption of the NIM in the SHG process and we have found that the conversion efficiencies remain high even for relatively high values of the absorption coefficient.

Although further material developments are still needed especially to minimize the losses present in currently available metamaterials, our results are very promising and point toward the possibility to achieve an additional whole new class of highly efficient harmonic generators based on NIM/PIM PBG structures.

One last note to point out is that in this work we have used the condition that the electric and magnetic plasma frequency are equal. This condition leads to equal permittivity and permeability in the NIM. Of course, in real metamaterials there can be in any case some discrepancy between the permittivity and permeability, nevertheless the optimal tuning conditions for SHG described in this paper may be achieved by varying, for example, the thickness of the layers and/or by varying the refractive index of the PIM.

## ACKNOWLEDGMENTS

Giuseppe D'Aguanno thanks the NRC for financial support.

[1] J. B. Pendry, Phys. Rev. Lett. **85**, 3966 (2000), and references therein.
[2] R. A. Shelby, D. R. Smith, and S. Schultz, Science **292**, 77 (2001).
[3] C. G. Parazzoli, R. B. Greegor, K. Li, B. E. C. Koltenbach, and M. Tanielian, Phys. Rev. Lett. **90**, 107401 (2003).
[4] V. G. Veselago, Sov. Phys. Usp. **10**, 509 (1968).
[5] G. D'Aguanno *et al.*, Opt. Lett. **30**, 1998 (2005).
[6] G. D'Aguanno *et al.*, Laser Phys. **15**, 590 (2005).
[7] M. J. Bloemer *et al.*, Appl. Phys. Lett. **87**, 261921 (2005).
[8] G. D'Aguanno, N. Mattiucci, M. Scalora, and M. J. Bloemer, Phys. Rev. Lett. **93**, 213902 (2004).
[9] I. Shadrivov, N. Zharova, A. Zharov, and Y. Kivshar,Opt. Express **13**, 1291 (2005).
[10] M. Scalora *et al.*, Phys. Rev. Lett. **95**, 013902 (2005).
[11] M. Marklund, P. K. Shukla, and L. Stenflo, Phys. Rev. E **73**, 037601 (2006).
[12] M. W. Feise, I. V. Shadrivov, and Yu. S. Kivshar, Appl. Phys. Lett. **85**, 1451 (2004).
[13] M. Lapine, M. Gorkunov, and K. H. Ringhoferi, Phys. Rev. E **67**, 065601(R) (2003).
[14] V. M. Agranovich, Y. R. Shen, R. H. Baughman, and A. A. Zakhidov, Phys. Rev. B **69**, 165112 (2004).
[15] I. V. Shadrivov *et al.*, J. Opt. Soc. Am. B **23**, 529 (2006); M. Scalora *et al.*, Opt. Express **14**, 4746 (2006).
[16] J. Li, L. Zhou, C. T. Chan, and P. Sheng, Phys. Rev. Lett. **90**, 083901 (2003).
[17] Yu Yuan *et al.*, Opt. Express **14**, 2220 (2006).
[18] I. V. Shadrivov, A. A. Sukhorukov, and Y. S. Kivshar, Appl. Phys. Lett. **82**, 3820 (2003).
[19] Haitao Jiang *et al.*, Appl. Phys. Lett. **83**, 5386 (2003).
[20] R. S. Hedge and H. G. Winful, Opt. Lett. **30**, 1852 (2005).
[21] G. D'Aguanno, N. Mattiucci, M. J. Bloemer, and M. Scalora, Phys. Rev. E **73**, 036603 (2006).
[22] N. Mattiucci, G. D'Aguanno, M. J. Bloemer, and M. Scalora, Phys. Rev. E **72**, 066612 (2005).

[23] R. W. Ziolkowski, Opt. Express **11**, 662 (2003).
[24] G. D'Aguanno, N. Mattiucci, M. Scalora, and M. J. Bloemer, Phys. Rev. E **71**, 046603 (2005).
[25] G. D'Aguanno, N. Mattiucci, M. Scalora, M. J. Bloemer, and A. M. Zheltikov, Phys. Rev. E **70**, 016612 (2004).
[26] S. Savasta, O. Di Stefano, and Raffaello Girlanda, J. Opt. Soc. Am. B **19**, 304 (2002).
[27] Podolskiy, A. K. Sarychev, and V. M. Shalev, Opt. Express **11**, 735 (2003).
[28] S. Linden *et al.*, Science **306**, 1351 (2004).
[29] Shuang Zhang *et al.*, Phys. Rev. Lett. **94**, 037402 (2005).
[30] Shuang Zhang *et al.*, Phys. Rev. Lett. **95**, 137404 (2005).
[31] C. Enkrich *et al.*, Phys. Rev. Lett. **95**, 203901 (2005).
[32] F. Garwe *et al.*, Proc. SPIE Int. Soc. Opt. Eng. **5955**, 59550T (2005).
[33] *Handbook of Optical Constant of Solids*, edited by E. D. Palik (Academic, New York, 1985).
[34] M. Scalora *et al.*, Phys. Rev. A **56**, 3166 (1997).
[35] M. Centini, C. Sibilia, M. Scalora, G. D'Aguanno, M. Bertolotti, M. J. Bloemer, and C. Bowden, Phys. Rev. E **60**, 4891 (1999).
[36] G. D'Aguanno *et al.*, J. Opt. Soc. Am. B **19**, 2111 (2002).